Journal of Russian Laser Research, Volume 28, Number 4, 2007

CHARACTERIZATION OF POLYCRYSTALLINE SILICON THIN FILMS FABRICATED BY EXCIMER LASER CRYSTALLIZATION

Chil-Chyuan Kuo

Department of Mechanical Engineering, Mingchi University of Technology
Gungjuan Road, 84, Taishan Taipei Hsien, 243, Taiwan, R.O.C
e-mails: jacksonk@mail.mit.edu.tw

Abstract

Phase transformation mechanisms during excimer laser crystallization and analysis of the resulting microstructures of polycrystalline silicon have been investigated in detail using in-situ time-resolved optical reflection and transmission measurements, field-emission scanning electron microscopy, high-resolution transmission electron microscopy, atomic force microscopy, and micro-Raman spectroscopy. Grain size, surface roughness, crystallinity, and melt-phase duration as functions of various excimer laser fluences are determined. A detailed microstructure development model of Si thin films upon complete melting using excimer laser irradiation is proposed. The results of this work can help in the development and fabrication of singular-grain Si thin film transistors.

Keywords: excimer laser crystallization, grain size, poly-Si, surface roughness, crystallinity, phase transformation mechanisms.

1. Introduction

In the past few years, excimer laser crystallization (ELC) has received considerable attention as a core technology for fabricating high-performance low-temperature poly-silicon thin-film transistors (LTPS TFTs) on non-alkaline glass substrate for advanced flat panel display applications [1–4]. However, some core issues affecting the quality of polycrystalline silicon (poly-Si) thin films such as surface roughness, crystallinity, grain size, structure defects, and cross-sectional microstructure analysis have not been explained satisfactorily. In this study, an in-situ time-resolved optical reflection and transmission (TRORT) [5] measurement system was developed to examine the melting and crystallization behavior of *a*-Si thin films during ELC on the basis of various excimer laser fluences, because the reflectivity and transmissivity are good probing indicators of the phase transformation of silicon thin films. After ELC, an extensive microstructural analysis of the resulting poly-Si films was performed by a field emission scanning electron microscopy (FE-SEM), micro-Raman spectroscopy, atomic force microscopy (AFM), and high-resolution transmission electron microscopy (HR-TEM).

Manuscript submitted by the author in English on May 1, 2007
1573-8760/07/2804-0383 ©2007 Springer Science+Business Media, Inc.

2. Experiment

Figure 1 is a schematic illustration of the experimental setup for measuring the melt-phase duration of molten Si during ELC. The sample had a stacked structure consisting of a 300-nm-thick SiO_2 capping layer and a 90-nm-thick *a*-Si layer formed on a 0.7-mm-thick non-alkali glass substrate (Corning 1737). These samples were then dehydrogenated by performing a thermal treatment at approximately 500°C for two hours to reduce the content of hydrogen for preventing the ablation caused by sudden hydrogen eruption during ELC. The sample was then held in self-closing tweezers at the end of the cantilever beam fixed on an $x - y$ precision translation stage. The x- and y-axis displacement of the two stages can accurately be controlled (resolution 0.625 mm) using a LabVIEW^{TM} (National Instruments Inc.) based custom design interface in order to yield large area crystallization. The movement of the focusing lens mounted on the z-axis stage was precisely controlled to adjust the excimer laser fluence during ELC. A power meter was used to calibrate the output excimer laser fluence. All the experiments were carried out under ambient conditions, using samples at room temperature.

Figure 1 shows a schematic diagram of the experimental setup for measuring the reflectivity and transmissivity during ELC. The *a*-Si thin films were irradiated by a XeF excimer laser beam ($\lambda = 351$ nm, repetition rate 1 Hz) with the excimer laser fluences ranging from 90 mJ/cm^2 to 350 mJ/cm^2. The excimer pulsed laser beam was not homogenized. The pulsed laser beam had a constant intensity profile in one direction but a Gaussian distribution in the orthogonal direction. The optical system was developed for ELC, which achieves the crystallization of silicon thin films with substrate temperature below 600°C. The excimer laser beam was reflected by a 45°-angle reflector and then focused on the sample using a focusing lens. During ELC, the TRORT measurements were performed using a continuous wave (CW) He–Ne probe laser (0.8 mW, TEM_{00}) operating at a wavelength of 632.8 nm. The time resolution was better than 1 ns and the relative measurement error on the time scale was less than 20%. The He–Ne laser had a 37° angle of incidence with respect to the sample surface and the laser beam was focused on the center of the laser-irradiated spot. The distance between the He–Ne probe laser and sample was approximately 300 mm. The transmitted and reflected beams from the sample were focused on the photodectors with response time in the nanosecond range. Interference filters were mounted in front of the photodetectors, allowing only red light from the He–Ne probe laser to contribute to the detected signal. A fast digital storage oscilloscope (bandwidth 500 MHz, sample rate 2 GHz/s) was used to record the reflection and transmission spectra. A beam splitter was used to reflect 10% of the XeF excimer laser beam to a photodetector for triggering the storage oscilloscope. The microstructures before and after ELC were analyzed by micro-Raman spectroscopy (Renishaw inVia), AFM, FE-SEM (JEOL JSM-6500F), and HR-TEM (JEOL JEM-2010).

Several samples were cross-sectioned for analysis by HR-TEM. Before FE-SEM observation, the crystallized silicon films were Secco-etched [6] (50% HF : H_2O : CrO_3 = 200 cc : 100 cc : 1.5 g) during 3 s in order to highlight the grain boundaries and intra-grain defects. The surface morphology was carried out using an AFM in tapping mode (scan rate 1 Hz). The rectangular Si tip was used as a probe with a spring constant of 40 N/m and was operated with a resonant frequency of 322.656 KHz. Raman spectroscopy was carried out using the backscattering geometry and a 514.5 nm Ar ion laser with a spot size of 5 μm. The full width at half maximum (FWHM) of the transverse optical (TO) Raman peak of Si(100) wafer was 4 cm^{-1}. It should be noted that the acceleration voltage for FE-SEM and HR-TEM were 15 and 300 kV, respectively. The structure parameters of poly-Si films obtained from various measurements are summarized in Table 1.

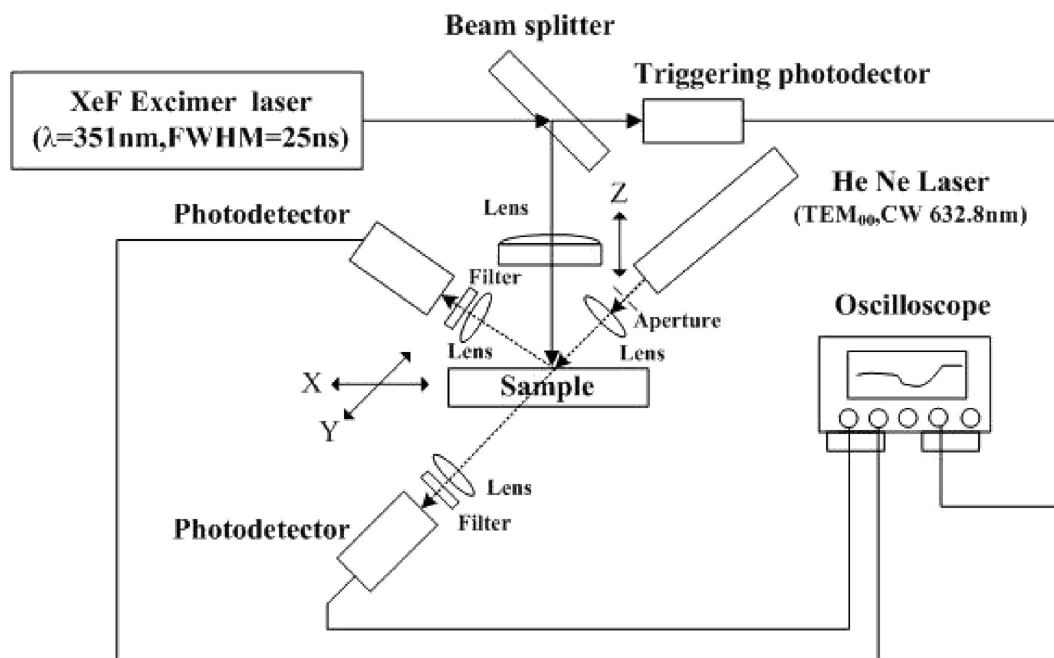

Fig. 1. Schematic diagram of the experimental setup for measuring reflectivity and transmissivity during ELC.

Table 1. Structure Parameters of Poly-Si Films Obtained from Various Measurements.

Measurement approach	Sample state	Structural parameters
FE-SEM	Secco-etched of poly-Si	Grain size/Grain shape
HR-TEM	A thin leaf of poly-Si	Grain size and shape/crystal orientation/ grain boundary shape
AFM	Poly-Si on the glass substrate	Surface roughness/surface morphology
Micro-Raman spectroscopy	Poly-Si on the glass substrate	Crystal volume fraction/intrinsic stress

3. Results and Discussion

The threshold laser fluence for surface melting associated with the amorphous Si to poly-Si transition is 100 mJ/cm^2 at room temperature. During ELC, the reflectivity signals increase because the molten Si acts like a highly reflective metallic liquid and the transmissivity signals decrease upon ELC. The transmissivity signal elucidates the phenomena exhibited by the complete Si thin films that undergo melting and resolidification during ELC. Figure 2 shows the TRORT spectra obtained from the partial melting laser fluence to the complete melting laser fluence. When the laser fluence exceeds the surface-melting threshold, poly-Si appears on the surface of the *a*-Si films. The width of the peak, defined as the duration of melting, increases as a function of the laser fluence [7].

The FE-SEM micrographs of the excimer laser-irradiated region with obvious grain boundaries, obtained by delineating defects using Secco-etching, show a high uniformity of poly-Si grains. Melt-phase

duration and grain size as a function of various excimer laser fluences is shown in Fig. 3. Two important observations can be inferred from this figure. First, the grain size depends sensitively on the incident excimer laser fluences within the narrow processing window. In the partial melting regime (100–180 mJ/cm^2), there is an increase in the grain size upon increasing the excimer laser fluences. Second, the longest melt-phase duration is approximately 119 ns at an excimer laser fluence of 200 mJ/cm^2, but the grain size is not at the maximum because of homogeneous random and dense nucleation by supercooling in the complete melting regime [1]. The grain size, however, reaches the maximum because of super lateral growth (SLG) nucleation in the near-complete melting regime at an excimer laser fluence of 190 mJ/cm^2. Indeed, a sudden increase in the melt-phase duration, which was observed at the transition from the low to high excimer laser fluence regime, is significantly indicative of the transition from partial melting and regrowth to complete melting of Si thin films. It is remarkable that the maximum size of the average grain reaches ∼1 mm.

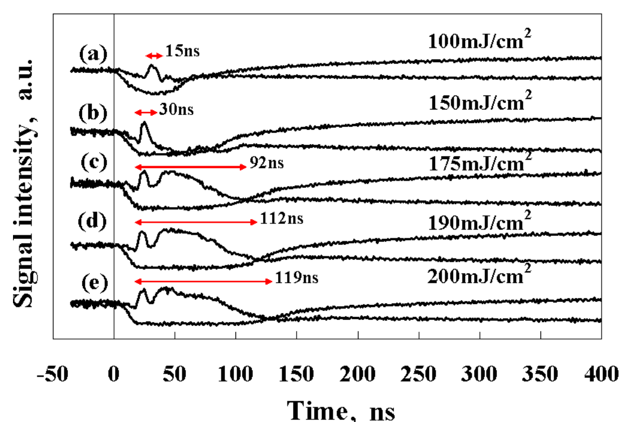

Fig. 2. TRORT spectra from the partial melting laser fluence to the complete melting laser fluence.

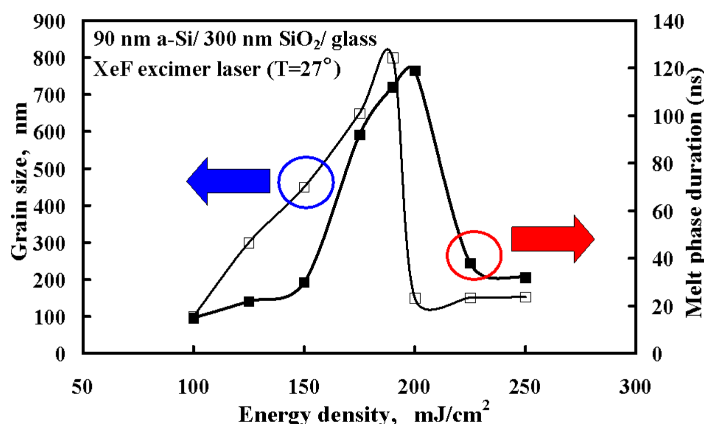

Fig. 3. Melt-phase duration and grain size as functions of excimer laser fluences. The diameter of the grain size was estimated from FE-SEM micrographs.

A corresponding FE-SEM micrograph for the Secco-etched film on glass is shown in Fig. 4. As can be seen, the defects decorated by Secco-etching are related to microtwins and low-angle grain boundaries (GBs), which can be attributed to the first-order phase transitions that occur in highly nonequilibrium conditions. This is confirmed by the corresponding HR-TEM micrograph, as shown in Fig. 5, which reveals microtwins in the sample. The disk-shaped crystal grain is also called radial-shaped crystal grain [8]. It should be noted that the microtwins significantly affect the electrical performance of LTPS TFTs. In the complete melting regime (200–225 mJ/cm^2), the disk-shaped microstructural feature was observed and was surrounded by the fine-grained poly-Si (smaller than 100 nm), which can be attributed to the fact that the supercooling associated with short pulses causes homogeneous random recrystallization from more nucleation sites [9].

Figure 6 shows a schematic diagram of a serious drawback of GBs caused by ELC. The field-effect mobility of the poly-Si TFTs fabricated by conventional ELC is approximately 100–200 cm^2/V·s [10], which limits the utilization of TFTs in other circuits, such as digital-to-analog converters and pixel memory. The limitation in the electron mobility is mainly caused by the fact that the trap states at the GBs are charged and form potential barriers. A number of carriers are generated from dense traps at the GBs, resulting in high leakage current under high drain voltage conditions. Ishihara et al. [11] proposed

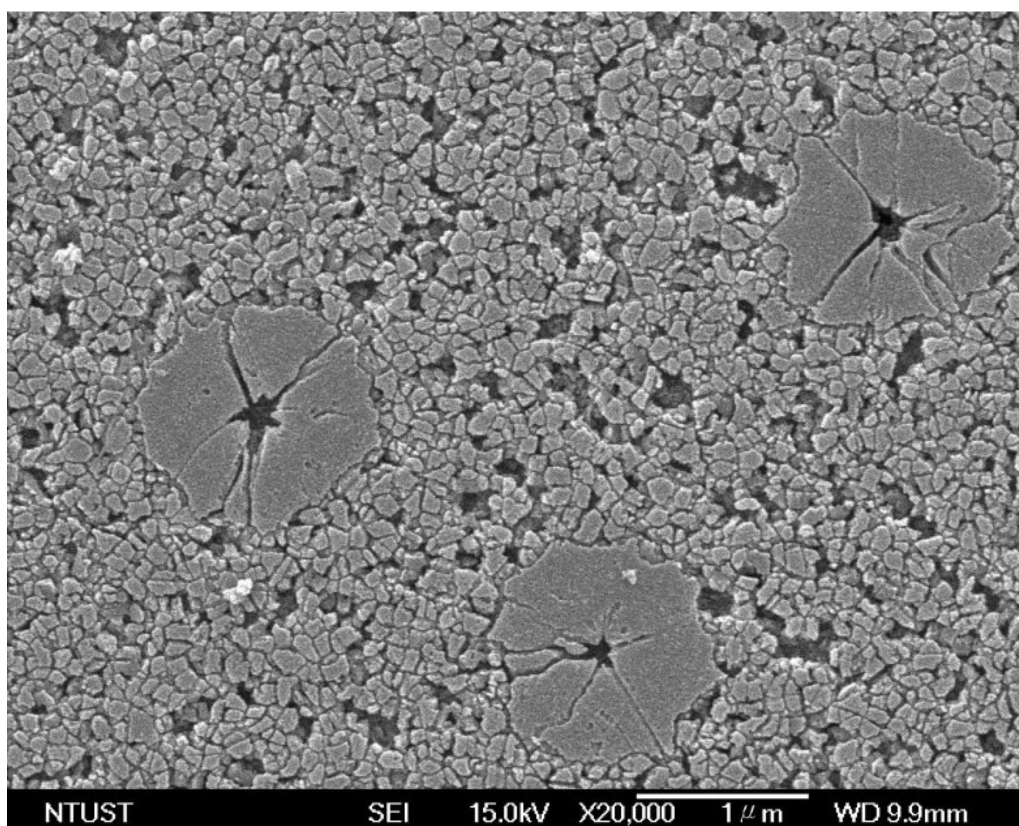

Fig. 4. FE-SEM micrograph of Secco-etched disk-shaped grains with a diameter of approximately 1 mm.

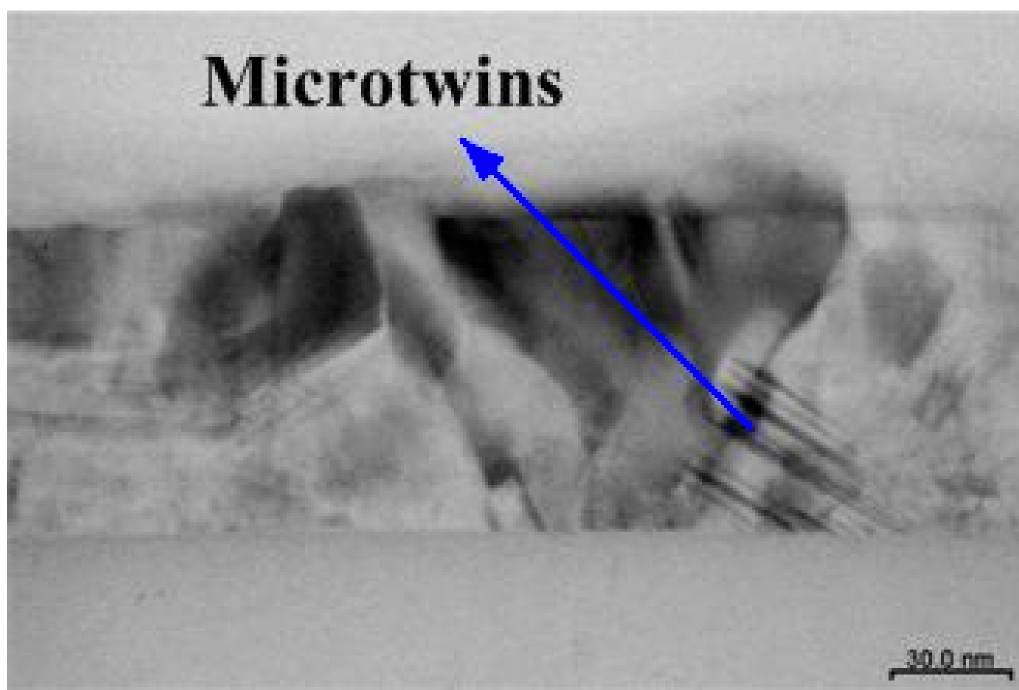

Fig. 5. HR-TEM micrograph of microtwins in the sample.

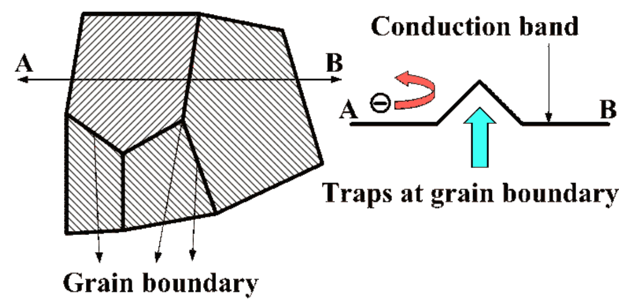

Fig. 6. Schematic illustration of the serious drawback of GBs caused by ELC.

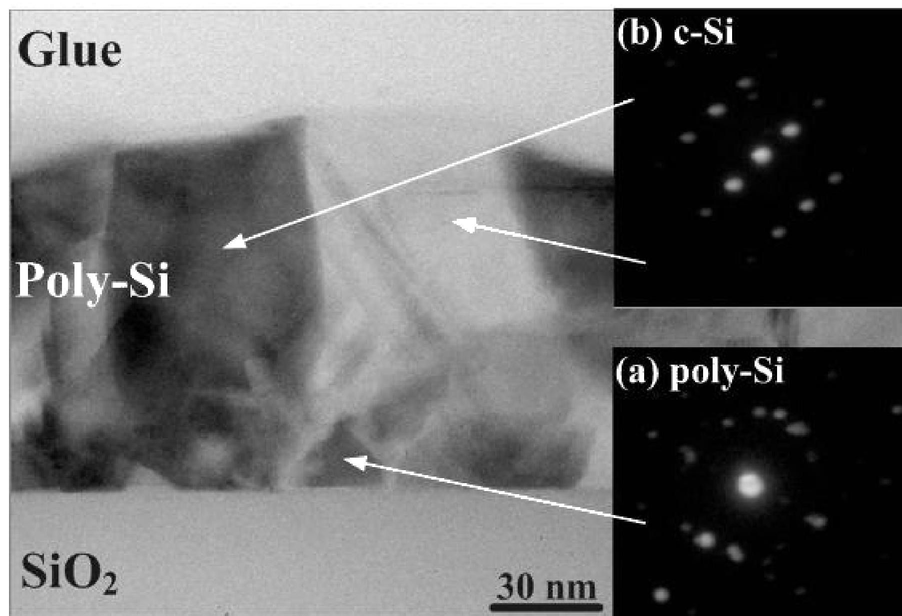

Fig. 7. Cross-sectional TEM micrographs of the microstructure after excimer laser crystallization with the corresponding SAD patterns for poly-Si (a) and *c*-Si (b).

that reduction of the number of GBs can improve both field-effect mobility and off-current. Accordingly, enlargement of the grain size is required for the fabrication of high-performance poly-Si TFTs using ELC.

A cross-sectional TEM micrograph of the crystallized microstructure is shown in Fig. 7, along with the selected area diffraction (SAD) patterns from *a*-Si and crystalline silicon (*c*-Si) regions of the sample. The SAD patterns reveal the crystallographic orientation of fine-grained (bottom of sample) and large-grained poly-Si (top of sample), respectively. As can be seen, it is apparent that the crystallinity of large-grained poly-Si is close to *c*-Si. According to TRORT measurements, and FE-SEM and HR-TEM observations, the details of the microstructure development model of Si thin films upon complete melting using excimer laser irradiation are summarized in Fig. 8. As can be seen, the solidification phenomenon of molten Si starts from the boundary between the irradiated spot and *a*-Si thin films by explosive crystallization (from point a to point b) [12] after complete melting using excimer laser irradiation, because the excimer laser spot is surrounded by *a*-Si thin films. Since the molten Si in the center of the irradiated spot remains at a high temperature, significant SLG recrystallization (from point b to

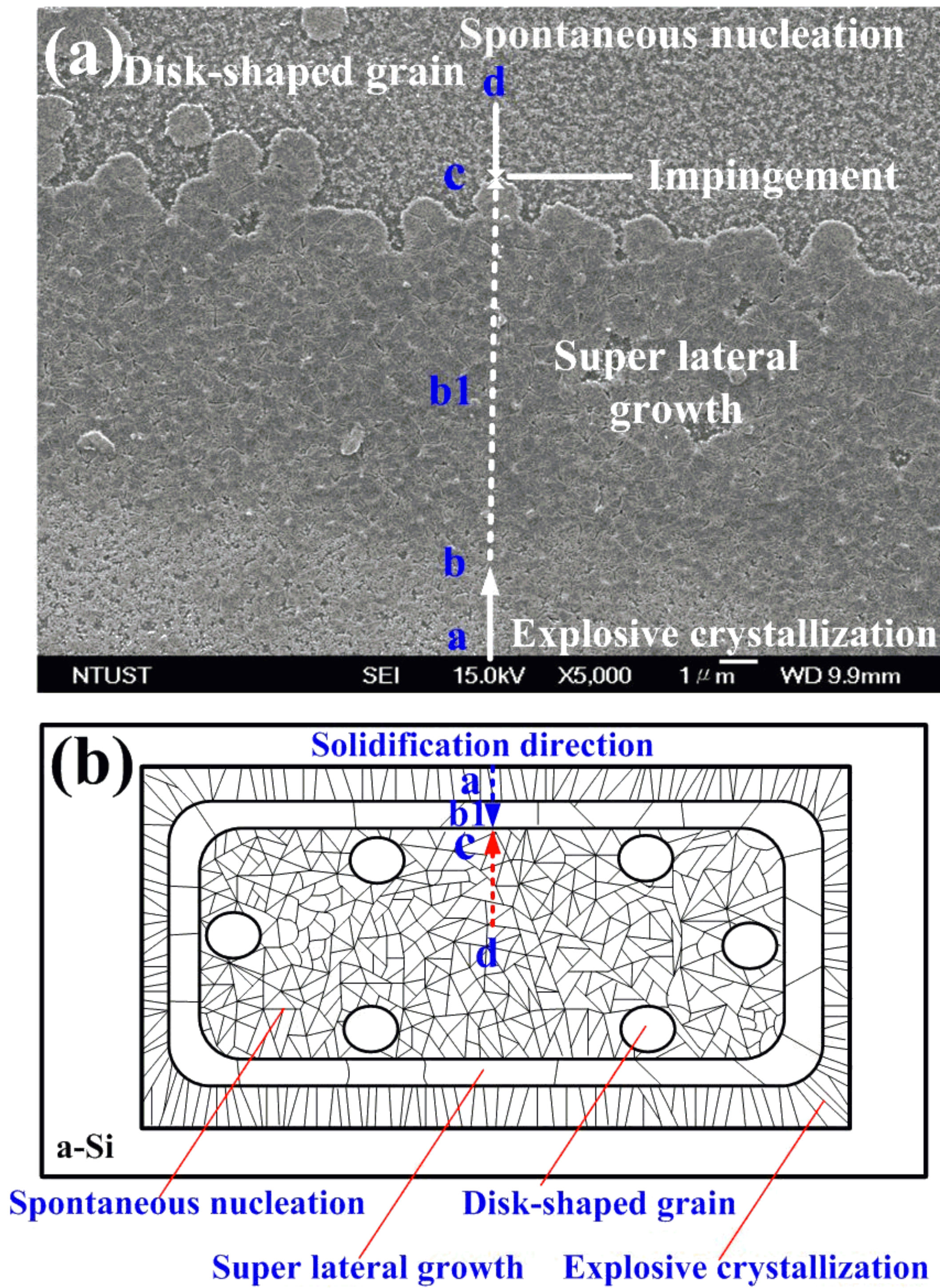

Fig. 8. Plane-view FE-SEM micrograph of Si thin films (a) and schematic illustrations of the microstructure development model (b). The arrow represents the solidification directions of poly-Si.

point c through route b_1) takes place and proceeds along the direction of the central molten Si until the impingement of the solidification fronts originating from the spontaneous nucleation [13] (from point d to point c). Some isolated disk-shaped grains are observed in the complete melting regime, which is caused mainly by the near complete melting recrystallization mechanism with the nucleation site forming unmelted residual Si underneath. In general, the grain sizes in the SLG regime are several times greater than the Si film thickness (90 nm). Experimentally, the maximum attainable grain size and diameter of grains in the SLG regime and disk-shaped grain in the complete melting regime are the same.

Figure 9 shows the surface topography of samples irradiated at laser fluence from partial melting to complete melting. A striking phenomenon observed in this figure is that the maximum roughness appears in the SLG regime (E = 190 mJ/cm^2). The fine-grained poly-Si films in the complete melting regime have a root mean square (RMS) roughness of 4–6 nm. The large-grained poly-Si films in the SLG regime have an RMS roughness of approximately 8.282 nm. This result indicates that a protrusive ridge is observed at this regime because a 10% density change between the solid (2.30 g/cm^3) and the liquid (2.53 g/cm^3) phases of Si films provides a driving force for the formation of capillary wave [14]. When the Si thin film is irradiated using excessive excimer laser fluence ($E >$ 250 mJ/cm^2), a fairly high surface roughness (RMS roughness = 38.98 nm) is observed, which shows that some Si thin film is evaporated after ELC. As can be seen, the surface roughness increases with the excimer laser fluence from 100 to 190 mJ/cm^2 due to significant mass transfer.

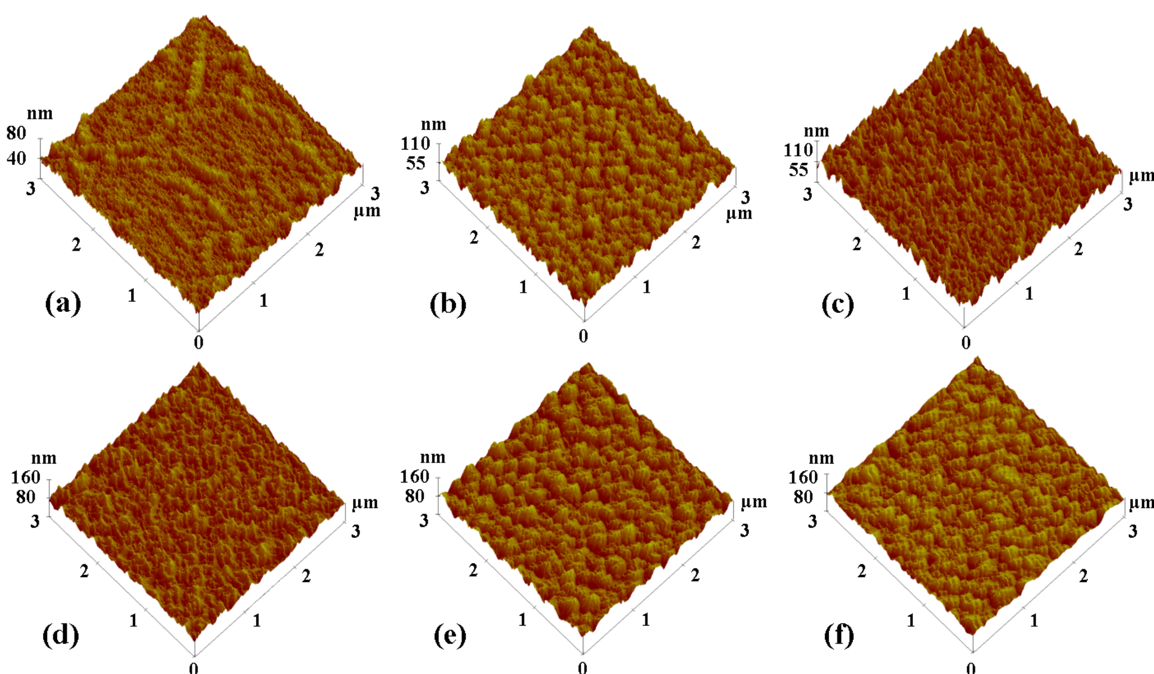

Fig. 9. Surface topography of samples irradiated at various laser fluences: 100 mJ/cm^2 (RMS=4.158 nm) (a), 130 mJ/cm^2 (RMS=6.771 nm) (b), 150 mJ/cm^2 (RMS=7.021 nm) (c), 175 mJ/cm^2 (RMS=7.9388 nm) (d), 190 mJ/cm^2 (RMS=8.282 nm) (e), and 200 mJ/cm^2 (RMS=6.552 nm) (f).

Figure 10 shows the micro-Raman scattering spectra of samples prepared by XeF excimer laser annealing with excimer laser fluence ranging from 100 to 225 mJ/cm^2. The Raman intensity increases at

first with excimer laser fluence and then saturates. The intensity, however, decreases at excimer laser fluences above 190 mJ/cm^2. On the other hand, the FWHM first decreases with excimer laser fluence and then increases. Figure 11 shows the FWHM of the micro-Raman scattering spectra for the poly-Si films obtained using laser fluence of 100–225 mJ/cm^2. The FWHM of the micro-Raman scattering spectra reaches a minimum level at excimer laser fluence of 190 mJ/cm^2. Such a difference can be attributed to grain size effects or to the existing internal strain [15]. The sharp peaks of the sample were centered in the range of 514–516 cm^{-1}. The crystallinity of ELC poly-Si films is approximately 100% because *a*-Si films were not observed in the micro-Raman scattering spectra, which is significantly different from that of poly-Si films made by solid phase crystallization [16]. This result reveals that ELC is a very powerful technology for producing crystallized poly-Si films by melt-mediated regrowth of Si films. These results are believed to give complementary information on the manufacturing of large-grained poly-Si films by ELC.

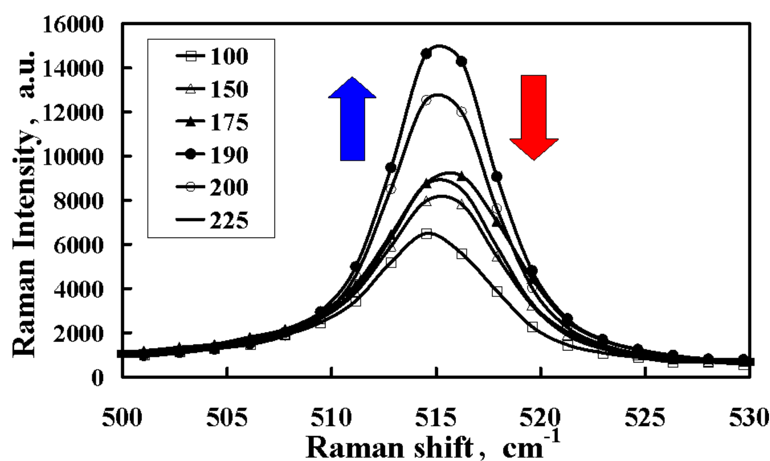

Fig. 10. Micro-Raman scattering spectra obtained using a laser fluence of 100–225 mJ/cm^2.

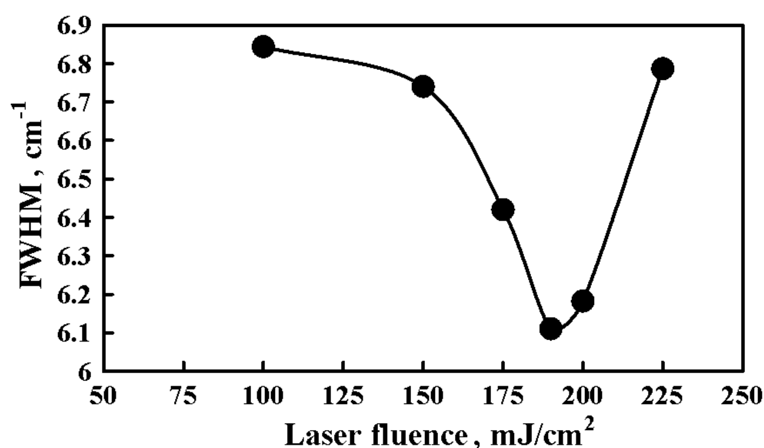

Fig. 11. FWHM of the micro-Raman scattering spectra obtained using a laser fluence of 100–225 mJ/cm^2.

4. Conclusions

The microstructure properties such as surface roughness, crystallinity, intra-grain defects, and grain size of poly-Si films were characterized by micro-Raman spectroscopy and AFM, HR-TEM, and FE-SEM observations. In-situ time-resolved optical diagnostics are effective for unraveling the phase transformation mechanisms during pulsed excimer laser annealing of Si thin films. ELC is a very promising technology for producing crystallized poly-Si films by melt-mediated regrowth of Si films with very high rates of heating and cooling. In general, uniform and large-grained poly-Si films with high crystallinity are required for fabricating high quality TFTs. It should be pointed out that the poly-Si films are free from structure defects such as high-angle GBs and microtwins, which can lead to high densities of the carrier trapping state. Indeed, poly-Si films with low-defect densities (microtwins or segregation) are not acceptable for fabricating single-grain (GBs free) Si TFTs [17] up to now. Solutions to this important issue by using heat-retaining thin films with suitable absorption coefficient in the sample have been carried out and will be presented in a future paper. The results reported here and the microstructure-development model proposed can serve as a good start point and have important applications for singular-grain Si TFT manufacturing in the near future.

Acknowledgments

The author thanks Prof. W. C. Yeh and Prof. J. Y. Jeng of the National Taiwan University of Science and Technology for stimulating discussions and assistance with the used experimental apparatus. The skillful technical assistance of Mr. C. P. Hsiao of the National Taiwan University of Science and Technology is highly appreciated.

References

1. J. S. Im, H. J. Kim, and M. O. Thompson, *Appl. Phys. Lett.*, **63**, 1969 (1993).
2. J. S. Im, M. A. Crowder, R. S. Spodili, et al., *Phys. Stat. Sol. (a)*, **166**, 603 (1998).
3. R. S. Sposili and J. S. Im, *Appl. Phys. Lett.*, **69**, 2864 (1996).
4. J. S. Im and H. J. Kim, *Appl. Phys. Lett.*, **64**, 2303 (1994).
5. C. C. Kuo, W. C. Yeh, C. B. Chen, and J. Y. Jeng, *Thin Solid Films*, **515**, 1651 (2006).
6. F. Secco d'Aragona, *J. Electrochem. Soc.*, **119**, 948 (1972).
7. D. H. Auston, C. M. Surko, T. N. C. Venkatesan, et al., *Appl. Phys. Lett.*, **33**, 437 (1978).
8. Y. Taniguchi, T. Katou, M. Hiramatsu, and M. Matsumura, *Jpn J. Appl. Phys.*, **45**, 7763 (2006).
9. S. R. Stiffler, M. O. Thompson, and P. S. Peercy, *Phys. Rev. Lett.*, **60**, 2519 (1988).
10. H. Kuriyama, S. Kiyama, S. Noguchi, et al., *Jpn J. Appl. Phys.*, **30** (1991).
11. R. Ishihara, M. He, V. Rana, et al., *Thin Solid Films*, **487**, 97 (2005).
12. M. O. Thompson, G. J. Galvin, and J. W. Mayer, *Phys. Rev. Lett.*, **52**, 2360 (1984).
13. S. R. Stiffler, M. O. Thompson, and P. S. Peercy, *Phys. Rev. B*, **43**, 9851 (1991).
14. D. K. Fork, G. B.Anderson, J. B. Boyce, et al., *Appl. Phys. Lett.*, **68**, 2138 (1996).
15. S. A. Lyon, R. J. Nemanich, N. M. Johnson, and D. K. Biegelsen, *Appl. Phys. Lett.*, **40**, 316 (1982).
16. T. Toyama, R. Muhida, T. Harano, et al., *Jpn J. Appl. Phys.*, **42**, L1347 (2003).
17. N. Higashi, G. Nakagawa, T. Asano, et al., *Jpn J. Appl. Phys.*, **45**, 4347 (2006).